~~On the r~~Relationship between wind observation accuracy and the ascending node of the sun-synchronous orbit for the Aeolus-type spaceborne Doppler wind lidar

Chuanliang Zhang[1,2], Xuejin Sun[2], Wen Lu[2], Yingni Shi[1], Naiying Dou[1], and Shaohui Li[1,2]

[1]Mailbox 5111, Beijing 100094, China

[2]College of Meteorology and Oceanography, National University of Defense Technology, Nanjing 211101, China

Corresponding to: Xuejin Sun (xuejin.sun@outlook.com)

Abstract. The launch and operation of first spaceborne Doppler wind lidar (DWL), Aeolus, is of great significance ~~in~~ to observing global wind field. Aeolus operates on ~~the~~ a sun-synchronous dawn-dusk orbit to minimize the negative impact of solar background radiation (SBR) on wind observation accuracy. ~~For that t~~F~~he f~~uture spaceborne DWLs may not operate on sun-synchronous dawn-dusk orbits due to their observation purposes.~~,~~ T~~t~~he impact of the local time of ascending node (LTAN) crossing of sun-synchronous orbits on the wind observation accuracy was studied in this paper by proposing two ~~added~~ given Aeolus-type spaceborne DWLs operated on the sun-synchronous orbits with LTANs of 15:00 and 12:00. On these two new orbits, the increments of the averaged SBR received by the new spaceborne DWLs range from 39 to 56 $\mathrm{mW\cdot m^{-2}\cdot sr^{-1}\cdot nm^{-1}}$ under cloud-free skies near the summer and winter solstices, which will lead to ~~the increment of averaged Rayleigh channel wind observation~~ uncertainties of 0.19 m/s and 0.27 m/s in the increment of the averaged Rayleigh channel wind observations for 15:00 ~~orbit~~ and ~~0.27 m/s for~~ 12:00 orbits ~~when~~ using the instrument parameters of ~~new spaceborne DWLs are the same with those of~~ Aeolus with 30 measurements per observation ~~with~~and 20 laser pulses per measurement. This demonstrates that Aeolus operating on the sun-synchronous dawn-dusk orbit is the optimal observation scenario, and the random error caused by the SBR will is larger on other sun-synchronous orbits. Increasing the laser pulse energy of the new spaceborne DWLs is used to lower the wind observation uncertainties. ~~Furthermore,~~And a method to quantitatively design the laser pulse energy according to the specific accuracy requirements is ~~given~~ proposed in this ~~paper~~ study based on the relationship between the signal~~-~~-to-noise ratio and the uncertainty of the response function of the Rayleigh channel. The laser pulse energies of the two new spaceborne DWLs ~~are~~ should be set to 70 mJ based on the statistical results ~~according to~~obtained using the method.~~,~~ ~~meanwhil~~The~~e~~ other instrument parameters ~~are~~ should be the same as those of Aeolus. Based on the proposed parameters ~~proposal~~, the accuracies~~y~~ of about 77.19% and 74.71% of the bins of the two new spaceborne DWLs would meet the accuracy requirements of the European Space Agency (ESA) for Aeolus~~, of which~~. These values are very close~~ly~~ ~~equivalent~~ to the ~~percentage of~~ 76.46% accuracy of Aeolus when ~~Aeolus are~~it is free of the impact of the SBR. ~~And~~ Moreover, the averaged uncertainties of the two new spaceborne DWLs in the free troposphere and stratosphere are 2.62 and 2.69 m/s ~~respectively~~, which perform better than that of Aeolus (2.77 m/s).

1 Introduction

The first spaceborne Doppler wind lidar (DWL) mission, the ~~ADM-Aeolus (ADM, ~~Atmospheric Dynamics Mission~~)~~ (ADM)-Aeolus, designed by the European Space Agency (ESA) was launched successfully on 22 August 2018~~, which~~. This mission has improved~~s~~ ~~people's ~~our knowledge ~~on ~~of the global wind field. Aeolus carries a spaceborne DWL, Atmospheric Laser Doppler Instrument (ALADIN), which has been used to make preliminary observations of the global wind field since ~~the ~~its launch. ~~And the first ~~Numerical Weather Prediction (NWP) experiments have shown that the assimilated wind observations have a significant positive impact on ~~the forecast of~~short-range wind, humidity and temperature ~~at short-range~~forecasts, especially in the tropical troposphere and the ~~south ~~South ~~hemisphere ~~Hemisphere (Straume *et al.*, 2019). Furthermore, scientists have also designed several possible observation scenarios ~~of ~~for future spaceborne DWLs. For example, c~~C~~onsidering that Aeolus ~~can ~~can only ~~realize the~~attain observations of single horizontal line-of-sight (LOS) wind components, Ma *et al.*~~,~~ (2015) and Masutani *et al.*~~,~~ (2010) proposed a spaceborne DWL concept with two pairs of telescopes (azimuth angles ~~from ~~of one pair ~~is ~~are 45° and 315°, and those of the other pair ~~is ~~are 135° and 225°) using both coherent-detection and direct-detection technology~~,~~; and ISHII *et al.*~~,~~ (2017) proposed ~~the ~~a spaceborne coherent DWL~~ concept~~ with one pair of telescopes (azimuth angles of 45° and 315°~~),~~). ~~both ~~Both of these~~ two ~~ observation scenarios can ~~provide~~detect the horizontal vector wind. In addition, Marseille et al. (2008) demonstrated that a larger observation coverage is more beneficial in the improvement of NWP results on~~in~~ global scale compared to the measurements of the horizontal vector wind by proposing several multi-satellite~~s~~ joint observation scenarios with Aeolus-type instruments. ~~However, the measurements of horizontal vector wind perform better for NWP results in the region close to the satellite tracks.~~Regarding multi-satellite joint observation scenarios, according to the World Meteorological Organization's (WMO) Observing Systems Capability Analysis and Review Tool (OSCAR) (Eyre, 2009), an observation cycle of 12 h with Aeolus operating on a sun-synchronous dawn-dusk orbit would meet "the minimum" requirements that have to be met to ensure the observations are useful for global NWP. When another Aeolus-type satellite operates on a sun-synchronous noon-midnight orbit combined with Aeolus, the observation cycle may become 6 h, which would meet breakthrough requirement that, if achieved, would result in a significant improvement in global NWP compared with those based on a single Aeolus.~~ In short, Aeolus is a demonstration mission which primarily aims to improve NWP and medium-range weather forecast, and there will be more observation scenarios of spaceborne DWLs with different observation purposes launched in the future.~~

Aeolus operates on ~~the ~~a sun-synchronous~~,~~ dawn-dusk orbit to minimize the impact of the solar background radiation (SBR) on the accuracy of the wind observations (Heliere *et al.*, 2002~~,~~; Baars *et al.*, 2019). In this study, ~~The ~~SBR is defined as the top-of-atmosphere (TOA) radiance ~~which ~~that is direct~~s~~ed toward the telescopes of the spaceborne DWL;~~s,~~ and the ~~the~~ solar background noise (SBN) is the photon counts excited by the SBR and imaged by~~on~~ the photon detectors (Zhang *et al.*, 2018), which ~~would ~~lowers the observation accuracy ~~by~~due to the Poisson noise (Liu *et al.*, 2006;~~,~~ Hasinoff *et al.*, 2010). The dawn-dusk orbit is ~~an~~ considered to be optimal ~~proposal to~~for lowering the impact of the SBR ~~for~~on spaceborne DWLs operating on sun-synchronous orbits. ~~The fu~~Future spaceborne DWLs may operate on different orbits ~~which should be related~~according to their observation purposes. ~~For example, according to Marseille et al. (2008), larger coverage of wind observations would perform better in improving results of NWP.~~According to experience gained from scatterometers used in global NWP (Stoffelen *et al.*, 2013), it has been demonstrated that the forecasting errors of tropical cyclone positions are much lower when the Indian Space Research Organisation's (ISRO) scatterometer, which has an ~12:00 UTC local overpass time, is assimilated in the NWP with the original METOP-A and METOP-B (~9:30 UTC local overpass time). ~~Furthermore~~Therefore, ~~if~~ it is assumed that if the global wind field at about 00:00/12:00 or 03:00/15:00 can also be observed, ~~we can reconstruct the wind speed diurnal cycle combing with the wind observations of Aeolus~~the global forecast may also be significantly improved. However, i~~I~~f the future spaceborne DWLs ~~would~~ operate on the sun-synchronous orbits ~~with different~~and the local time of ascending node (~~local time of ascending node (LTAN) crossing~~LTAN) crossing differ, the received SBR would become larger, which would lead to higher uncertainties of the wind observations.

Aeolus is a direct-detection Doppler wind lidar that senses the winds through a Mie channel and a Rayleigh channel. A~~A~~ccording to the technology mechanism of Aeolus, the factors that affect the ~~observations~~ accuracy of the wind observations of spaceborne DWLs include atmospheric heterogeneity~~,~~ and SBR~~, et al~~. The ~~Aeolus is a direct-detection Doppler wind lidar which senses winds through Mie channel and Rayleigh channel. Mie channel senses winds using the laser signal backscattered from aerosol/cloud particles, and Rayleigh channel sensing winds using molecular backscatter signal.~~ a~~A~~tmospheric heterogeneity mainly affects the wind observations ~~on~~of the Mie channel, which senses the wind using the laser signal backscattered from the aerosol/cloud particles. Sun *et al*~~.~~,. (2014) ~~indicate~~reported that typical values for wind uncertainties ~~on~~for the Mie channel in the free troposphere caused by atmospheric heterogeneity are in the range of 1–1.5 m/s ~~caused by atmospheric heterogeneity~~, which cannot be easily corrected. ~~And f~~For the Rayleigh channel, the uncertainties caused by atmospheric heterogeneity ~~range between~~are 0.2–~~ and~~ 0.6 m/s in the troposphere, which can be largely reduced ~~by~~using a scene classification algorithm. The SBR mainly affects the observations ~~on~~ obtained by the Rayleigh channel, which senses the wind using molecular backscatter signals.~~,~~ The~~and~~ SBR has less impact on the observations ~~in~~ obtained by the Mie channel (Rennie, 2017). ~~The study of~~ Zhang *et al.*, (2019) ~~illustrates~~ demonstrated that the received SBR of Aeolus ranges from 0 to 169 mW·m^{-2}·sr^{-1}·nm^{-1}. ~~And w~~When the SBR is greater than 80 mW·m^{-2}·sr^{-1}·nm^{-1}, the ~~whole profiles of~~entire wind observation profiles ~~would be~~is less accurate.

~~The o~~Observations of the global winds would improve the results of NWPs.~~,~~ H~~h~~owever, ~~tif~~ the assimilation of ~~observations of~~ low accuracy observations ~~are assimilated, the~~ has a negative impact on the NWP results ~~would be introduced~~ (Stoffelen *et al.*, 2005, 2006). According to the accuracy requirements of the ESA, the uncertainties of the horizontally projected line-of-sight (HLOS) wind observations in the Planetary Boundary Layer (PBL), free troposphere, and stratosphere should be less than 1, 2, and 3 m/s, respectively (Stoffelen et al., 2005). ~~And t~~The latest research has also demonstrated that the uncertainties of 1 m/s in the PBL, 2.5 m/s in the free troposphere, and 3–~~∼~~5 m/s in the stratosphere would also ~~allow~~ have significant positive impacts ~~o~~in the NWP results (Straume *et al.*, 2019). The heights of the boundar~~y~~ies between the PBL, free troposphere, and stratosphere are 2 km and 16 km, respectively. In this paper, we assume~~d~~ that ~~the~~ an accuracy of 5 m/s in the stratosphere ~~was~~ is required. The free troposphere ~~mentioned below specially~~is hereinafter referred to as the ~~free~~ troposphere.

Assuming that ~~the~~ future Aeolus-type spaceborne DWLs ~~will~~ would operate on ~~the~~ sun-synchronous orbits with different LTANs, the distributions of the received SBR near the winter and summer solstices and the corresponding uncertainties of the wind observations caused by the SBR were ~~figured out~~determined in this paper. ~~The~~ A method ~~to~~ of lowering the uncertainty to a specific accuracy level, ~~i.e~~that is. to meet the accuracy requirements of the ESA, or to reach ~~the similar~~ an accuracy level similar to that of Aeolus~~,~~ was also ~~discussed~~developed. In general, the only way to reduce the effect of the Poisson noise ~~was~~ is to capture more signal (Vahlbruch *et al.*, 2008). According to the L~~l~~idar equation, the following methods can be used to increase the return signal energy of spaceborne DWLs: 1) increasing the laser pulse energy; 2) lowering the height of the orbits; 3) enlarging the telescope aperture; and 4) reducing the vertical resolution (Marseille and Stoffelen, 2003). ~~In addition, the~~The orbit height of Aeolus was adjusted from the originally designed 400 km to 320 km to increase the energy of the received signal. In this paper, the ~~increasing~~ laser pulse energy was ~~used~~ increased to lower the uncertainty. The remainder of this paper is organized as follows~~–~~. ~~The~~ The details of the orbits of the three spaceborne DWLs and the Aeolus-type spaceborne DWL simulation system are presented in Sect~~.~~ion 2. Section 3 ~~gives~~ describes the ~~a~~ method ~~to~~of quantitatively design~~ing~~ing the laser pulse energy of spaceborne DWLs based on specific accuracy requirements. Before th~~at~~is, the relationship between the signal-to-noise ratio (SNR) and the uncertainty of the response function of the Rayleigh channel ~~is also~~are discussed. In Sect~~.~~ion 4, ~~the~~ a preliminary proposal ~~of~~ for laser pulse energ~~y~~ies of the two new spaceborne DWLs is presented based on~~given using~~ the method ~~mentioned~~described in Sect~~.~~ion 3 ~~based on~~, the global distributions of SBR and wind observation uncertainties, ~~as well as~~and the accuracy requirements for spaceborne DWLs. Sect~~.~~ion 5 presents the summary and conclusions.

2 ~~The s~~Sun-synchronous orbits and simulation system of spaceborne DWLs

In general, for sun-synchronous orbits, ~~the~~ a spaceborne DWL ~~running~~ operating on ~~the~~ a dawn-dusk orbit (LTAN of 18:00) would receive the minimum amount of SBR, and ~~the~~ a spaceborne DWL ~~running~~ operating on ~~the~~ a noon-midnight orbit (LTAN of 12:00) would receive the maximum amount of SBR. In order to study the impact of the orbit selection on the accuracy of the wind observation~~s accuracy~~, ~~the~~ spaceborne DWLs operating on three sun-synchronous orbits with LTANs of 18:00, 15:00, and 12:00 ~~respectively were~~ are proposed. ~~And th~~Thee simulation system used to calculate the uncertainty of the wind observations ~~was~~ is also described.

2.1 ~~The s~~Sun-synchronous orbits

The three sun-synchronous orbits with LTANs of 18:00, 15:00, and 12:00 are illustrated in Fig. 1~~ ~~(a). Aeolus, which operating on the sun-synchronous~~,~~ dawn-dusk orbit with height of 320 km, is marked in blue. The spaceborne DWL is equipped with a single-perspective telescope, which ~~scanning~~ scans at 90° with respect to the satellite track, ~~under~~ has a slant angle of 35° versus the nadir, and ~~measuring~~ measures the profiles of the HLOS wind components. The other two spaceborne DWLs ~~running~~ operating on ~~the~~ sun-synchronous orbits with LTANs of 15:00 and 12:00 ~~which~~ are marked in yellow and red~~ lines~~, respectively. The intersection points between the laser beam and the E~~e~~arth's surface are called the off-nadir points ~~of which lines~~and are illustrate in Fig. 1(b).

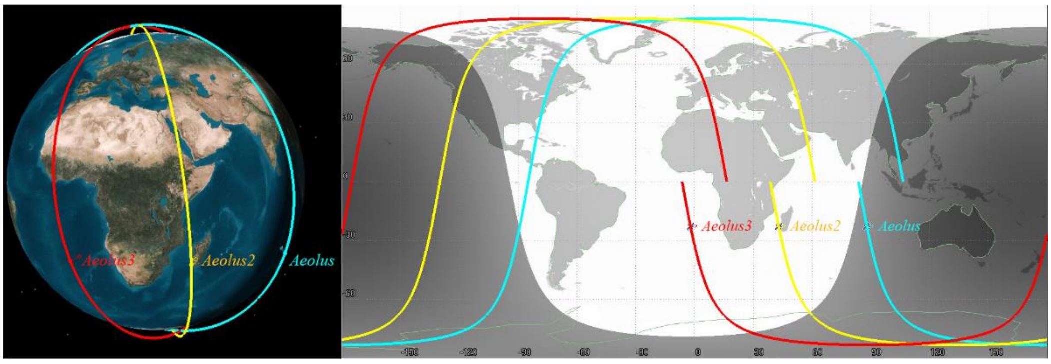

Figure 1. The orbits of the spaceborne DWLs operating on the sun-synchronous orbits with LTANs of 18:00, 15:00, and 12:00~~, which~~ are marked in blue, yellow, and red, respectively. (a) 3D graphics; (b) 2D graphics.

The two new spaceborne DWLs are assumed to be Aeolus-type instruments ~~whose~~ with the same instrument parameters ~~the same as those~~as of Aeolus, except ~~different~~ their laser pulse energies, which ~~aims~~ are altered to improve the ~~wind observation~~ accuracies of their~~y~~ wind observations. The ~~When demonstrating the instrument parameters of spaceborne DWLs, people also pay attention to the observation accuracy under worst cases. s~~Solar zenith angle is the dominant factor for the SBR received by spaceborne DWLs. The variations ~~of~~in the solar zenith angles of the off-nadir points on the three orbits within one ~~-~~year~~ range~~ are illustrated in Fig. 2.~~,~~ ~~which indicates~~This shows that the received SBR ~~would~~ reaches the maximum values near the summer ~~solstice~~ and ~~reach maximal values near~~ winter solstices. For the off-nadir points, in the ~~north~~ North H~~h~~emisphere, the SBR will reach the maximum near summer solstice~~.~~, ~~And SBR~~whereas it will reach the maximum near the winter solstice ~~for the off-nadir points~~ in the S~~s~~outh H~~h~~emisphere. In this paper, ~~When demonstrating the instrument parameters of spaceborne DWLs, people also~~we ~~pay attention to~~focused on the observation accuracy under the worst ~~cases~~SBR conditions. ~~the~~ The global distributions of the maximum SBR in a 1°×1° grid near the summer solstice ~~which range from~~ (June 14 to 28) and near the winter solstice ~~which ranges from~~ (December 15 to 30) ~~are~~were used for the investigations~~ of the worst cases with maximum Rayleigh channel wind observation uncertainties due to SBR~~. Furthermore, the annual variation characteristics of the solar zenith angles are less obvious ~~on~~ for the two new orbits compared to ~~that~~ those of Aeolus ~~as shown in~~ (Fig. 2), which indicates that the observations of the two new spaceborne DWLs would ~~–~~more ~~likely~~ frequently ~~to~~ encounter~~suffer~~ the wors~~t~~e case~~s~~ SBR conditions on the Rayleigh channel compared ~~to that of~~with Aeolus.

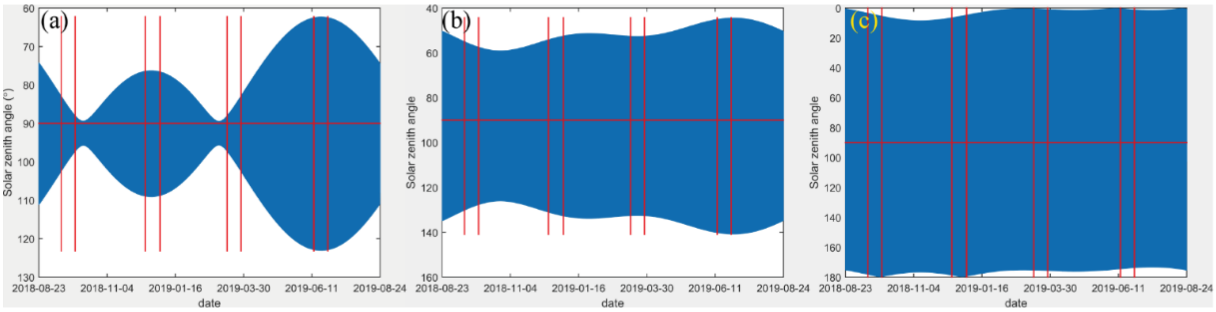

Figure 2. The variations ~~of~~ in solar zenith angles of the off-nadir points on the three orbits within one -year ~~range~~. The 4 time ranges divided by 8 red lines denote 15 days near the autumn equinox, winter solstice, spring equinox and summer solstice, respectively. Sun-synchronous orbits with LTANs of 18:00 (a), 15:00(b), and 12:00(c).

2.2 Spaceborne DWL simulation system

~~An Aeolus-type spaceborne DWL simulation system c~~Considering the impact of the SBR on the wind observation uncertainties, an Aeolus-type spaceborne DWL simulation system was developed ~~-was developed~~ to ~~retrieve HLOS wind components and~~ calculate the observation uncertainties. The simulation system was built according to the optical structure of Aeolus.~~,~~ ~~which~~It consists of a laser transmitter, ~~the~~ a telescope and front optics, a Mie spectrometer, a Rayleigh spectrometer, and front detection ~~front~~ units (Marseille and Stoffelen, 2003~~-and~~; Paffrath, 2006). Considering that the SBR mainly affects the observation accuracy of the Rayleigh channel, we focused on the simulation of the wind retrieval~~ed~~ method on the Rayleigh channel~~,~~ and assumed that the cross-talk effect between the Mie channel and the Rayleigh channel is negligible. The details of the working principle and the instrument parameters for~~of~~ Aeolus used in the simulation system, expect for the laser pulse energy, were set according to the ADM-Aeolus Algorithm Theoretical Basis Document (ATBD) Level 1B products (Reitebuch *et al.*, 2018)~~,~~ ~~expect laser pulse energy which is set to 60 mJ, which was consist with the laser pulse energy of onboard Aeolus~~. ~~-In addition, i~~In the simulation system, one observation consists~~ed~~ of 30 accumulations (also called 30 ~~-as~~ measurements), and one measurement consists of 20 shots, resulting in an average horizontal ~~averaging~~ length of about 90 km per observation. The d~~D~~etection chain noise of 4.7 e$^-$/pixel on the Rayleigh channel for each measurement was also ~~taken into account~~consiedered. The vertical resolutions of the retrieved wind were 500 m in the PBL, 1 km in the troposphere, and 2 km in the stratosphere (Marseille et al., 2008).

The input parameters of the simulation system included the u- and v- components of the wind, temperature, pressure, aerosol optical properties, and TOA radiance. In this paper, the impacts of the SBR on the wind observation accuracy of the spaceborne DWLs under cloudy ~~atmosphere~~ conditions were not considered. The first five components were derived from the pseudo-truth global atmospheric condition dataset, which consistes~~d~~ of the Ozone Monitoring Instrument (OMI) database (McPeters *et al.*, 2008), including the latitude-averaged profiles of the temperature, pressure, and density of ozone, and the lidar climatology of vertical aerosol structure for spaceborne lidar simulation studies (LIVAS) database (Amiridis *et al.*, 2015), which was used to describe the aerosol optical properties. Only the aerosols in the PBL were considered here. The details used to derive the global distributions of the SBR received by Aeolus-type spaceborne DWLs ~~could refer to~~have been described by

Zhang *et al.* (2019), which wereand thus only briefly introduced here. First, the positions of the off-nadir points of the spaceborne DWLs were obtained using satellite orbit simulation software. The aAtmospheric conditions were retrieved from the pseudo-truth databases and were spatially interpolated to the off-nadir points. The surface albedo was is also needed to generate the TOA radiance, which was derived from the database of lambert-equivalent reflectivity (LER) database (Koelemeijer *et al.*, 2003). Then, the SBR of the off-nadir point was generated by using the radiative transfer model (RTM) libRadtran with the input of atmospheric optical properties, and surface albedo (Emde *et al.*, 2016). Finally, the earth Earth was divided into 1°×1° grids, and the maximum SBR in each grid is picked outwas selected as the worst cases conditions offor the Rayleigh channel wind observation uncertainties due to the SBR. Once the atmospheric conditions and SBR were input tointo the simulation system, the HLOS winds and their corresponding uncertainties in the grids could be figured outwere determined.

3 Methodology

In this study, a mMethod of increasing the laser pulse energies of Aeolus-type spaceborne DWLs was used developed to lower wind observation uncertainties in this paper. To assess the performance of the spaceborne DWLs under worst case conditionss of the Rayleigh channel, and quantitatively design the laser pulse energies of two new spaceborne DWLs as mentioned in Sect.ion 2.1, we take the steps are as follows:. 1) the The global distributions of the maximum SBR received by the spaceborne DWLs on the three orbits were figured outdetermined to compare the SBR received by the two new spaceborne DWLs with that of Aeolus;. 2) the The uncertainties of the wind observations on of the Rayleigh channel of the three spaceborne DWLs were derived, and the uncertainty increments of the uncertainties of the two new spaceborne DWLs were compared to that those of Aeolus were figured out;. 3) tThe relationship between the wind observation uncertainty and the laser pulse energy was established.; 4) TThe values of the laser pulse energies which that would lower the uncertainties to the required accuracy level were derived based on the relationship established in sthe step 3).

3.1 Uncertainty of the wind observations on of the Rayleigh channel

The double-edge technique is was used to retrieve the HLOS wind components on of the Rayleigh channel for Aeolus (Flesia and Korb, 1999;, Zhang et al., 2014). The study of Tan *et al.*, (2008) showeds that the uncertainty on of the Rayleigh channel is determined by the response function, temperature, and pressure. A Llookup table between for the wind speed, and response function, temperature, and pressure is was established prior to the launch of Aeolus. In operation mode, the profiles of temperature and pressure profiles arewere obtained from the European Centre for Medium-Range Weather Forecasts' (ECMWF) data assimilation system. Once the response function of the Rayleigh channel is detected by spaceborne DWL, the wind speed will can be figured outretrieved. The uncertainty of the wind observation is estimated as

$$\sigma_{v_{HLOS}} = \frac{\partial v_{HLOS}}{\partial R_{ATM}} \sigma_{R_{ATM}}, \tag{1}$$

where $\sigma \cdot$ ~~denotes~~ is the uncertainty~~,~~; $\partial \cdot$ ~~denotes~~ is the partial derivative. v_{HLOS} ~~means~~ is the HLOS wind component. R_{ATM} ~~means~~ is the response function of the Rayleigh channel which is defined as

$$R_{ATM} = \frac{N_A - N_B}{N_A + N_B}, \tag{2}$$

where N_A and N_B are the useful signals detected by the Rayleigh channel.

~~The~~ $\partial v_{HLOS}/\partial R_{ATM}$ is a function of temperature and pressure, ~~which~~ and it ranges from 420 to 520 m/s ~~upon~~ on most occasions~~, as shown in~~ (Fig. 1 of Zhang et al., ~~(~~2019). The uncertainty of the response function is ~~derived from~~

$$\sigma_{R_{ATM}} = \frac{2}{(N_A + N_B)^2} \sqrt{N_B^2 \sigma_A^2 + N_A^2 \sigma_B^2}, \tag{3}$$

where σ_A and σ_B ~~denote~~ are the uncertainties of N_A and N_B, respectively. Here, N_A and N_B can be obtained using the simulation system of the spaceborne DWLs. Taking the SBR and the noise of the spaceborne DWL detectors into account, according to the features of the Poisson noise, the uncertainties in N_A and N_B can be estimated as follow:

$$\sigma_A^2 = N_A + N_{S,A} + N_{noise}^2, \text{ and } \sigma_B^2 = N_B + N_{S,B} + N_{noise}^2, \tag{4}$$

where the $N_{S,A}$ and $N_{S,B}$ are the photon counts ~~which are~~ excited by the SBR ~~on~~for the Rayleigh channel. N_{noise} ~~denote~~is the noise of the detection unit ~~on~~for Rayleigh channel.

$N_{S,A}$ and $N_{S,B}$ can be derived using the following method.~~:~~ T~~t~~he SBR is viewed as a~~the~~ spectrum ~~following~~with ~~the~~a uniform distribution, and ~~of which~~its energy can be obtained using Eq. (5) (Nakajima *et al.*, 1999)~~,~~. ~~and t~~The bandwidth is equal~~s~~ to that of the interference filter of the Rayleigh channel. $N_{S,A}$ and $N_{S,B}$ can be obtained from the simulation system ~~with the input of~~when the spectrum is input.

$$S_{SBR} = nE_Q E_O L_S \varphi_R \frac{A_r^2 \cdot \pi}{4} \Delta\lambda \Delta t, \tag{5}$$

where S_{SBR} ~~denotes~~ is the energy of the SBR;~~,~~ n ~~denotes~~ is the number of ~~the~~ accumulated laser shots~~,~~; E_Q and E_O ~~denote~~ are the quantum efficiency of the detector ~~on~~ of the Rayleigh channel (Reitebuch *et al.*, 2018)~~;~~, and L_S ~~denotes~~ is the TOA radiance of the off-nadir point. As ~~to~~ for the instrument parameters, φ_R ~~denotes~~ is the field of view; A_r ~~denotes~~ is the diameter of the telescope; and $\Delta\lambda$ ~~denotes~~ is the bandwidth of the interference filter. ~~–~~Δt denotes the laser detection time, which ~~was~~ is dependent on the vertical resolution.

3.2 Relationship between uncertainty and laser pulse energy

The laser pulse energy of the laser transmitter has an important influence on the uncertainty of the wind observation. Provided that the atmospheric conditions remain unchanged, the higher the laser energy, the stronger the backscattered signal received by the telescope of the Aeolus-type instrument ~~will become stronger~~, and the smaller the influence of the corresponding Poisson noise ~~will be smaller~~, which will finally lower the uncertainty of the wind observations ~~finally~~. However, the quantitative relationship between the laser pulse energy and the wind observation uncertainty ~~is~~ has not yet derived due to the fact that the wind observation uncertainties are affected by various factors such as the atmospheric conditions and instrument parameters. In this ~~paper~~study, ~~the~~ a method ~~for~~ of quantitatively deriv~~ation~~ ing of the laser pulse energy according to the specific wind observation accuracy requirement~~s of wind observation~~ is ~~proposed~~developed ~~through~~by establishing the relationship between the SNR of the Rayleigh channel and the uncertainty of the response function of the Rayleigh channel.

According to the characteristics of the Poisson noise, Marseille and Stoffelen, (2003) defined the SNR of the Rayleigh channel:~~.~~

$$SNR_{Ray} = \frac{N_A+N_B}{\sqrt{N_A+N_B+N_{S,A}+N_{S,B}+2N_{noise}^2}}. \tag{6}$$

For the Rayleigh channel of a spaceborne DWL, the difference between N_A and N_B is not large, especially when the wind speed is close to zero, that is, $N_A \approx N_B$. Based on the assumption that $N_A \approx N_B$ and $N_{S,A} \approx N_{S,B}$, we derived the relationship between the SNR and the uncertainty of the response function of the Rayleigh channel:~~.~~

$$\sigma_{R_{ATM}} \approx \frac{1}{SNR_{Ray}}. \tag{7}$$

The details of the derivations and the proofs are ~~shown~~ presented in the Appendix. Then, the uncertainty of the wind observations ~~on~~ from the Rayleigh channel can be estimated as

$$\sigma_{v_{HLOS}} \approx \frac{\partial v_{HLOS}}{\partial R_{ATM}} \cdot \frac{1}{SNR_{Ray}}. \tag{8}$$

~~While increasing~~When the laser pulse energy is increased, the value of $N_A + N_B$ will increase proportionally ~~increase~~.~~;~~ S~~s~~imilarly, $N_{S,A} + N_{S,B}$ will increase proportionally ~~increase with~~as the ~~increase of~~ SBR increases, which can be written as

$$E_{laser} \propto N_A + N_B, S_{SBR} \propto N_{S,A} + N_{S,B}. \tag{9}$$

According to Eqs. (6) and (8), ~~setting~~ $x = N_A + N_B$, which is in proportional to the energy of the laser pulse E_{lasr}; $y = N_{S,A} + N_{S,B}$, which is in proportional to the energy of the SBR S_{SBR};~~,~~ and $z = \sigma_{HLOS}$;~~,~~ $f(T,P) = \partial v_{HLOS}/\partial R_{ATM}$ and~~,~~ $C = 2N_{noise}^2$, where T ~~denotes~~ is temperature and P ~~denotes~~ is pressure. Thus,~~,~~ the relationship between x, y, and z can be expressed as

$$z \approx f(T,P)\frac{\sqrt{x+y+C}}{x}. \tag{10}$$

Equation (10) can be solved as follows:

$$x \approx \frac{f^2(T,P)+f(T,P)\cdot\sqrt{f^2(T,P)+4z^2(y+C)}}{2z^2}. \tag{11}$$

Equation (10) illustrates that the uncertainty is determined by temperature, pressure, variable x, the SBR, and dark noise of the detector. The value of x can be estimated using Eq. (11). Knowing the value of x, the value of the laser energy cannot be ~~figured out~~determined ~~for that~~because the variable x is dependent on the laser energy and the wind speed. However, when the wind speed ~~keeps~~ remains unchanged, the variable x ~~would be in~~is proportional to the energy of the laser pulse E_{laser}. That is~~ to say~~, if the laser energy increases by several times, the corresponding value of the variable x will increase by the same multiple~~s~~ when the HLOS wind speed ~~keeps~~ remains unchanged. Then, the required value of the laser energy can be obtained based on the proportional relationship between x and E_{laser}.

3.3 Derivation of laser pulse energy

In Section~~.~~ 3.2 and the Appendix, the relationship between the laser pulse energy E_{laser} and the wind observation uncertainty was established based on ~~some~~several assumption and simplifications. The following method was used to solve the problem ~~that~~of how ~~much~~high to set the laser energy ~~could be set~~ to increase the accuracy of the observations of the new spaceborne DWLs to the meet specific accuracy requirements.

First~~ly~~, the laser pulse energies of the two new spaceborne DWLs were assumed to be 60 mJ, and the ~~of which~~ parameters are the same as those of Aeolus~~;~~. T~~t~~he profiles of the uncertainties were derived using simulation system based on the global distributions of the maximum SBR for~~on~~ the three orbits~~; secondly,~~. Second, the profiles of variable x at each bin (layer, the concept ~~can~~ refers to Fig. 5 in Tan et al., ~~(~~2008~~)~~) were ~~figured out~~determined using Eq. (11), ~~which~~ and they were set as $x1$. ~~Provided~~ Assuming that the accuracy requirements of the two new spaceborne DWLs are ~~to~~ that their accuracies reach the accuracy level of Aeolus, then~~,~~ the uncertainties of the new spaceborne DWLs were replaced with the uncertainties of Aeolus at the same bins, and the variables of $f(T,P)$, y, and C were kept ~~unchanged~~the same.~~,~~ T~~t~~he variables x were ~~figured out~~determined using Eq. (11), ~~which~~ and they were set as $x2$.~~;~~ F~~f~~inally, according to the proportional relationship between x and the laser energy, $E_{new}/E_{Aeolus} \approx x2/x1$, the required laser pulse energy at each bin ~~could be~~was derived. Therefore, we could determine the laser energies of the two new spaceborne DWLs according to the statistical results.

In the same way, if the accurac~~y requirements~~ies of the two new spaceborne DWLs were required to meet the accuracy requirements of the ESA, we needed to replace the wind observation uncertainties when the laser energy was 60 mJ with the accuracy requirements of the ESA when calculating the values of $x2$, and the other steps ~~were~~ are the same as above.

4 Results and discussion~~s~~

The preliminary results ~~to~~ of ~~determine~~ the laser pulse energies of the two new spaceborne DWLs ~~were~~ are presented in this section. To obtain the laser pulse energies, first the global distributions of the maximum SBR ~~on~~ of the three orbits and the corresponding wind observation uncertainties caused by the SBR ~~were~~are calculated, firstly. Then, the distributions of the required laser energies ~~we~~are obtained according to the accuracy requirements based on the method ~~mentioned~~described in S~~ubs~~ect~~.~~ion 3.3. Finally, based on these results, the propos~~al of~~ed laser pulse energies of the two new spaceborne DWLs are~~was~~ presented. T~~And t~~he global distributions of wind observation uncertainties of the three spaceborne DWLs ~~were figured out~~are determined according to the new ~~instrument parameter proposal~~laser pulse energies. The details ~~were shown~~are provided in the following subsections.

4.1 Global distributions of the maximum SBR ~~on~~ of the three orbits

The g~~G~~lobal distributions of the maximum SBR received by the spaceborne DWLs ~~running~~operating on the three orbits in summer and winter are shown in Fig. 3 based on the instrument parameters of Aeolus and the three orbits ~~mentioned~~ described in Sect~~.~~ion 2.

The contours in Fig. 3 denote the differences between the SBRs of the two new orbits and sun-synchronous dawn-dusk orbit, which demonstrates that the dawn-dusk orbit is ~~an effective solution~~the optimal observation scenario ~~to~~ for minimizinge received SBR for Aeolus-type spaceborne DWLs operating on sun-synchronous orbits. ~~While~~ When operating on ~~the~~ a sun-synchronous dawn-dusk orbit, the maximum SBR of the off-nadir points located in the ~~southern~~ Southern ~~hemisphere~~ Hemisphere is nearly equal to zero in summer, and the maximum SBR of the off-nadir points located in the ~~northern~~ Northern H~~h~~emisphere is nearly equal to zero in winter. For the two new orbits, almost all of the wind observations ~~of~~in a few areas are not affected by the SBR, which are mainly located in the regions near the Antarctic and Arctic circles. According to the contours, the order of ascending ~~order of the values of~~ maximum SBR, ~~on~~ the three orbits ~~is~~ are dawn-dusk orbit, the orbits with an LTAN of 15:00, and ~~that~~ of the orbit with an LTAN of 12:00 respectively. The closer the LTANs of the orbits are to noon, the larger the values and the ~~affected~~ area affected ~~of~~by the SBR ~~will~~ become ~~larger~~. The sS~~tatistics~~tatistics illustrate that the average~~d~~ SBR values of the dawn-dusk, 15:00, and 12:00 orbits illustrated in Fig. 3 are 20.99, 60.68, and 76.36 mW·m^{-2}·sr^{-1}·nm^{-1}, respectively, near the summer and winter solstice periods. The averaged increments of the SBR received by new spaceborne DWLs are 60.68-20.99=39.69 mW·m^{-2}·sr^{-1}·nm^{-1} and 76.36-20.99=55.37 mW·m^{-2}·sr^{-1}·nm^{-1} ~~compared to~~higher than that of Aeolus, respectively.

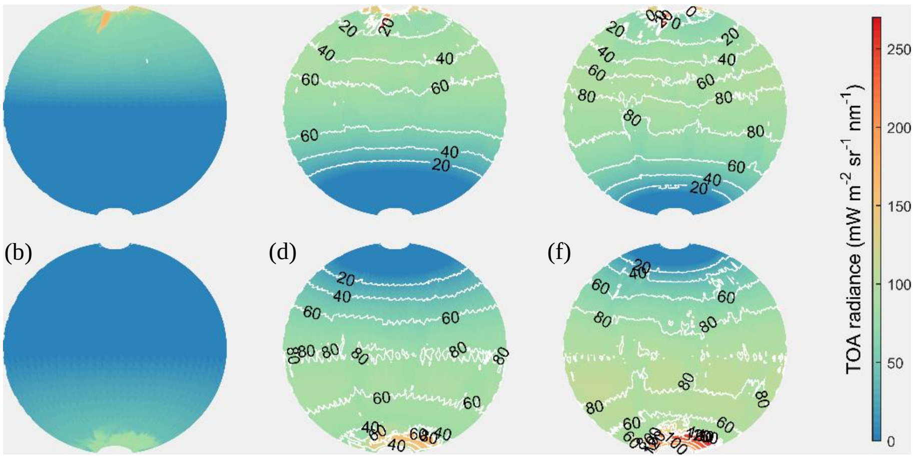

Figure 3. The g~~G~~lobal distributions of the maximum SBR received by spaceborne DWLs operating on the three orbits. Fig~~s~~. 3(a, b), 3(c, d) and 3(e, f) present the sun-synchronous orbits with LTANs of 18:00, 15:00, and 12:00 respectively, and the upper panels denote the SBR in summer, and the lower panels denote the SBR in winter. The contours in the Fig~~s~~. 3(c, e), 3(d, f) denote the differences between the SBR in Fig~~s~~. 3(c, e), 3(d, f) with the SBR in Fig~~s~~. 3(a, b), respectively.

4.2 Uncertainties of wind observations based on the instrument parameters of Aeolus

Figure 3 illustrates~~d~~ the global distributions of the maximum SBR near the summer and winter solstice~~ periods~~s, which ~~paid more attention to~~focus on the worst SBR cases ~~of~~ for the Rayleigh channel wind observation uncertainties. In fact, for sun-synchronous orbits, nearly half of the off-nadir points ~~would be~~are in darkness, ~~which would~~so they are ~~be~~ free of the impact of the SBR, ~~and~~ while the other half ~~would be~~are in daylight and are affected by the SBR. ~~As to~~For the off-nadir points in darkness, the latitude-averaged global distributions of the wind observation uncertainties for Aeolus-type instruments ~~, in latitude-averaged were~~ are shown in Fig. 4.

Figure 4 illustrates that~~:~~ 1) w~~W~~ithout the impact of SBR, most of the wind observations in the free troposphere and stratosphere ~~would~~ meet the accuracy requirements of the ESA. The bins for~~of~~ which the uncertainties ~~are beyond~~exceed the requirements of the ESA are mostly located in the upper layer of troposphere and stratosphere. In addition, the accuracy of the wind observations in the PBL is relatively low~~, which~~ and basically ~~cannot~~ does not meet the requirements of the ESA. In fact, the Mie channel is mostly used for wind observations due to the widespread presence of aerosols in the PBL. Therefore, the accuracy of the Rayleigh channel in the PBL is not considered in the following section of this paper. The s~~S~~tatistics show that the average~~d~~ uncertainties without the impact of the SBR are all about 2.61 m/s in summer and winter, and overall, about 76.46% of the bins ~~would~~ meet the accuracy requirements of the ESA~~ overall~~.

2) Without the impact of the SBR, the wind observation uncertainties ~~have little differences among~~are very similar at different latitudes.

3) The wind observation uncertainties increase with atmospheric altitude~~s~~ when the heights of the range gates ~~are~~ remain unchanged. This is mainly due to the fact that the molecular number density is proportional to the pressure. Near the height of 16 km, the uncertainties decrease ~~first~~ initially and then increase with~~ the~~ increas~~es i~~ing altitude, which is attributed~~s~~ to the change in the thickness of the bins from 1 km to 2 km.

4) Compared with other regions, the uncertainties in the equatorial region are higher at the bottom of the troposphere~~,~~ and are lower in the stratosphere. The trend of the temperature profile in the equatorial region is the main reason for this phenomenon, which is consist with the trend of the uncertainties. The n~~N~~umber density of molecules is inversely proportional to the temperature. A l~~L~~ow molecular number density leads to a weak return signal of spaceborne DWLs, which leads to higher wind observation uncertainties.

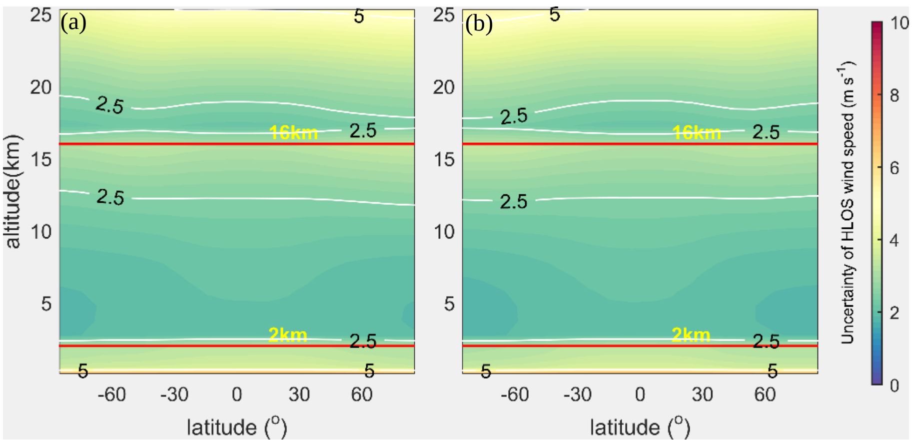

Figure 4. The latitude-averaged global distributions of the wind observation uncertainties ~~in latitude-average~~ without the impact of the SBR. (a) summer; (b) winter.

Based on the global distributions of the maximum SBR of the three orbits illustrated in Fig. 3, the worst SBR cases of for the Rayleigh channel with maximum wind observation uncertainties due to SBR were also derived as shown in (Fig. 5). Considering that the distributions of the maximum SBR were are nearly horizontal to the latitudes, and in to simplify the calculations, Fig. 5 was obtained using the 10 ° latitude-averaged SBR and atmospheric conditions.

As can be seen by comparingComparisons between Fig. 4 and Fig. 5, illustrate thatthe wind observation uncertainties become larger with as the impact of the SBR increases. And tThe uncertainties show exhibit obvious characteristics of latitudinal variations., whichThis is mainly attributed to the latitudinal variations of in the maximum SBR shown in Fig. 3. As the LTANs of the orbits get closer to noon, the wind observation uncertainties gradually increases, so doand the number of bins of whichthat do not accuracy cannot meet the accuracy requirements of the ESA also increases. For the bins in the troposphere and stratosphere, about 71.35% can meet the accuracy requirements of the ESA for Aeolus, ; while the percentages are 63.45% for the orbit of 15:00 orbit and 60.67% for the orbit of 12:00 orbit. The averaged uncertainties of the three spaceborne DWLs in the troposphere and stratosphere are 2.77, 2.96, and 3.04 m/s respectively, which illustrates that the increments in averagedof the average uncertainties of the Rayleigh channel on of the new orbits are about 3.25-3.06=0.19 m/s and 3.32-3.06=0.27 m/s larger than that of Aeolus. Considering that the impact of the SBR on the wind observations is minimal on dawn-dusk orbit, and reaches the maximum on noon-midnight orbit, the phenomenon indicates the selection of the LTANs of sun-synchronous orbits will make the global average wind observation uncertaintiesleads to a maximum a maximum difference of 0.27 m/s in average global wind observation uncertainties for the Rayleigh channel of Aeolus-type DWLs near the summer and winter solstices. This small degradation of the uncertainties could also be used as an argument for operating Aeolus-type spaceborne DWLs on other sun-synchronous orbits rather than a dawn-dusk orbit. In addition, the average global averaged uncertaintiesty without impact of SBR is 2.61 m/s without impact of the SBR as Fig. 4 indicates;, and the average global averaged uncertaintiesy is 3.04 m/s under the worst SBR casess offor the Rayleigh channel on the orbit with LTAN of 12:00. Thise comparison illustrates that SBR causesd athe maximum increase in the averaged wind observation uncertainty of about 3.04-2.61=0.43 m/s for Aeolus-type DWLs operating on the sun-synchronous orbits.

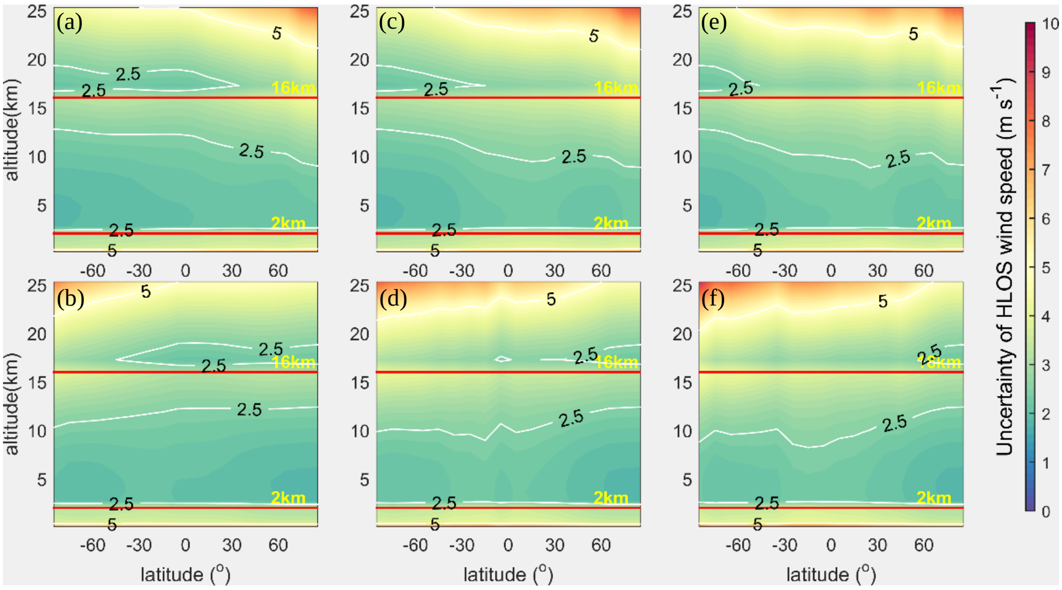

Figure 5. The zonal distributions of the Rayleigh channel wind uncertainties in clear air conditions observed by the three spaceborne DWLs operat~~ed~~ing on the three orbits of which the instrument parameters are the same as those of Aeolus. The contours show the accuracy requirements of ESA. The arrangement of the subgraphs corresponds to that of Fig. 2.

4.3 Distribution~~s~~ of the required laser pulse energy

In order to make the accurac~~y~~ies of the two new spaceborne DWLs ~~to~~ reach the specific accuracy level under the worst SBR case~~s~~ for the ~~of~~ Rayleigh channel, the required laser pulse energies were obtained using the method ~~mentioned~~ described in Sect~~.~~ion 3.3. According to Eq. (11), the required energy ~~is determined by~~ depends on the temperature, pressure, wind uncertainties, SBR, and noise of the instrument, and thus, the required laser pulse energy is different in different bins. Therefore, the laser pulse energies of the new spaceborne DWLs should be determined by the statistics of the profiles of their required energ~~y~~ies.

~~Supposed~~ Assuming that the wind observation accuracy of the two new spaceborne DWLs ~~is required~~ needs to reach the accuracy level of the Aeolus as is ~~as~~ shown in Figs. 5(a, b), which can be used for joint observations of the three satellites, the global distributions of the required laser pulse energies ~~are~~ were derived and are illustrated in Fig. 6~~, which~~. Fig. 6 ~~illustrates~~ shows that for of the most bins of the two new spaceborne DWLs, it is necessary to increase the laser pulse energy if the accuracy of the wind observations is expected to reach the accuracy level of Aeolus. Especially in the equatorial region, a higher laser pulse energy is needed.

~~Statistics reveal that the averaged values of required laser pulse energies in Fig. 6 is 64.80 mJ for the 15:00 orbit, and 66.59 mJ for the 12:00 orbit respectively. The quantiles of the required energy of the two spaceborne DWLs are shown in Table 1, which means that the corresponding percentages of the bins whose accuracy will reach the accuracy level of Aeolus once the laser pulse energies equal to the specific values. For example, 90% of the bins will reach or exceed the accuracy level of Aeolus when the laser energy is 70.37 mJ for the spaceborne DWL operating on the 15:00 orbit. As we can see from Table 1, when the instrument parameters of two new spaceborne DWLs are the same as Aeolus, of which the laser pulse energies are equal to 60 mJ, only the accuracy of about 20% of the bins can reach the accuracy level of Aeolus near summer and winter~~

~~solstices. However, as long as the laser energy is slightly increased, the percentages of bins will greatly increase. When the laser pulse energies reach 70 mJ, the accuracy of about 90% of bins could reach or exceed the accuracy level of Aeolus on the orbit 15:00, and the percentage is about 80% on the orbit 12:00.~~

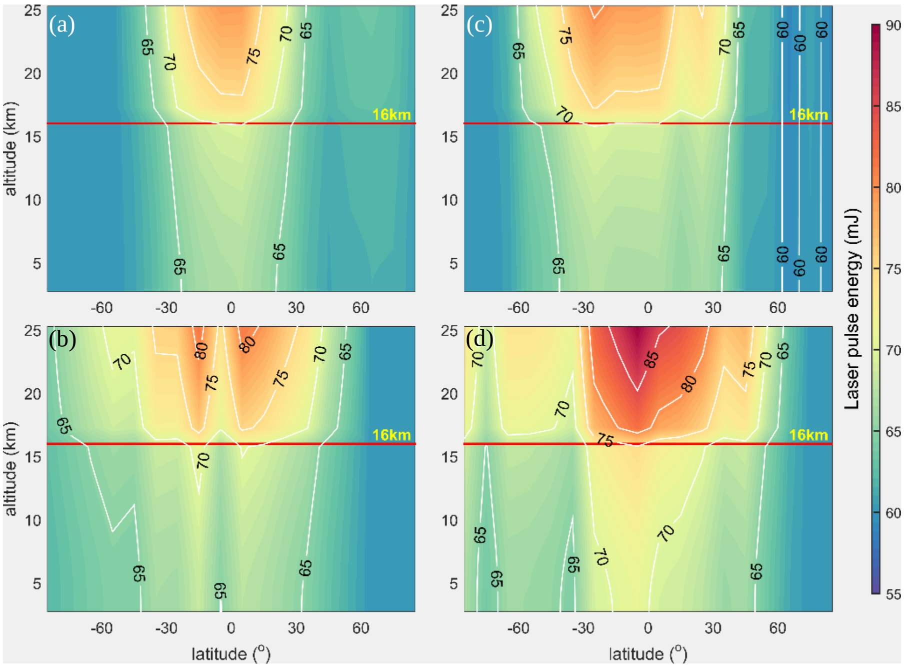

Figure 6. The ~~G~~global distributions of the required laser pulse energies in troposphere and stratosphere to make the ~~the wind observation~~ accuracies~~y~~ of the two new spaceborne DWLs reach the accuracy level of the Aeolus. Fig~~s~~. 4(a, b) and (c, d) denote the sun-synchronous orbits with LTANs of 15:00 and 12:00 respectively. The upper panels denote the distributions in summer, and the lower panels denote the distributions in winter.

Table 1. The q~~Q~~uantiles of the required laser pulse energies of the two new spaceborne DWLs to reach the accuracy level of Aeolus.

Quantile (%)		20	40	50	60	70	80	90	100
Required energy	Orbit 15:00	60.62	62.53	64.00	65.26	66.54	67.85	70.37	81.68
(mJ)	Orbit 12:00	60.71	65.04	66.47	67.34	68.59	70.59	73.74	89.78

The statistics reveal that the average values of the required laser pulse energies in Fig. 6 are 64.80 mJ and 66.59 mJ for the 15:00 and 12:00 orbits, respectively. The quantiles of the required energies of the two spaceborne DWLs are shown in Table 1, which shows the corresponding percentages of the bins in which the accuracy reaches the accuracy level of Aeolus once the laser pulse energies are equal to the specific value. For example, 90% of the bins will reach or exceed the accuracy level of Aeolus when the laser energy is 70.37 mJ for the spaceborne DWL operating on the 15:00 orbit. As can be seen from Table 1, when the instrument parameters of the two new spaceborne DWLs are the same as those of Aeolus, i. e., laser pulse energies of 60 mJ, the accuracies of only about 20% of the bins reach the accuracy level of Aeolus near the summer and winter solstices. However, when the laser energy is slightly increased, the percentages of the bins greatly increases. When the laser pulse energy reaches 70 mJ, the accuracies of about 90% and about 80% of the bins reach or exceed the accuracy level of Aeolus on the orbit 15:00 and 12:00 orbits, respectively.

Another potential application of the new spaceborne DWLs is to enlarge the global wind observation coverage to improve the forecast results of NWPs. ~~It is supposed to~~This should have a positive impact on the NWP results ~~once~~ when the wind observation accuracy meets the requirements of the ESA. The distributions of the ~~required~~ laser pulse energies of the three orbits required to meet the accuracy requirements of the ESA are illustrated in Fig. 7.

~~Figure 7 illustrates that the wind observation uncertainties of most bins in the low level of troposphere and stratosphere can meet the accuracy requirements of ESA for the three spaceborne DWLs with the laser pulse energy of 60 mJ. Higher energies are needed in the upper level of troposphere and stratosphere, especially for the regions close to Antarctic and Arctic circles. On the boundary line with height of 16 km, there is an obvious sudden decrease in required laser energies. This is mainly because the vertical thickness of observation bins changes from 1 km in the troposphere to 2 km in the stratosphere, which makes the integration time of detection units of Rayleigh channel double. And larger atmospheric backscattered signal will be integrated. On the other hand, the required wind observation uncertainties increase from 2 m/s to 3 m/s. Therefore, the required laser energies reduce suddenly when going from troposphere to stratosphere near the height of 16 km. Comparisons among the required laser energies of the three orbits illustrate that the closer the orbital LTANs are to noon, the averaged values of the required laser energies will become larger. Statistics show that the averaged values of required energies are 53.27 mJ for Aeolus, 57.60 mJ for the 15:00 orbit, and 59.19 mJ for the 12:00 orbit respectively. The quantiles of the required energies of the three spaceborne DWLs are shown in Table 2. The statistics of Table 2 illustrate that the percentages of bins which can meet the accuracy requirements of ESA increase by 10% even if the laser pulse energy is not increased much when quantile is between 40% to 90%. The averaged increment of laser pulse energy is 6.75 mJ which can increase the quantiles by 10% considering the three orbits as a whole. When the laser pulse energies are set to 67.89, 73.71, and 75.98 mJ, the quantiles will be up to be 80%, which exceeds the percentage of bins (76.46%) for Aeolus without the impact of SBR.~~

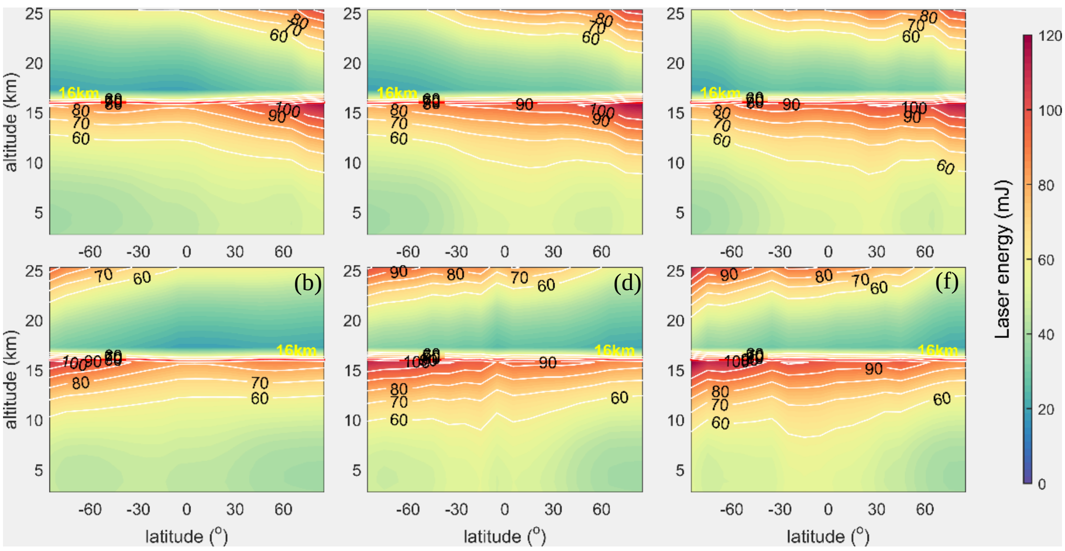

Figure 7. The g~~G~~lobal distributions of the required laser pulse energies in the troposphere and the stratosphere to reach the accuracy requirements of the ESA. The arrangement of the subgraphs corresponds to that of Fig. 2.

Table 2. The q~~Q~~uantiles of the required laser pulse energy of the three spaceborne DWLs to meet the accuracy requirements of the ESA.

Quantile (%)		20	40	50	60	70	80	90	100
Required energy (mJ)	Orbit 18:00	40.93	46.33	49.35	53.87	59.22	67.89	78.63	116.96
	Orbit 15:00	42.83	50.88	53.17	58.21	63.96	73.71	84.88	118.20
	Orbit 12:00	45.06	51.81	54.76	59.86	66.46	75.98	86.82	121.19

Figure 7 illustrates that the wind observation uncertainties of most of the bins in the lower level of the troposphere and the stratosphere meet the accuracy requirements of the ESA for the three spaceborne DWLs with a laser pulse energy of 60 mJ. Higher energies are needed in the upper level of the troposphere and the stratosphere, especially in for the regions close to the Antarctic and Arctic circles. On the boundary line with height of 16 km, there is an obvious sudden decrease in the required laser energies. This is mainly because the vertical thickness of the observation bins changes from 1 km in the troposphere to 2 km in the stratosphere, which doubles the integration time of the detection units of Rayleigh channel. Larger atmospheric backscattered signal will be integrated. Moreover, the required wind observation uncertainties increase from 2 m/s to 3 m/s. Therefore, the required laser energies suddenly decrease when transitioning from the troposphere to the stratosphere near a height of 16 km. The comparison of the required laser energies of the three orbits illustrates that the closer the orbital LTANs are to noon, larger the average values of the required laser energies will become.The statistics show that the average values of the required energies are 53.27 mJ for Aeolus, 57.60 mJ for the 15:00 orbit, and 59.19 mJ for the 12:00 orbit. The quantiles of the required energies of the three spaceborne DWLs are shown in Table 2. The statistics presented in Table 2 illustrate that the percentages of the bins that meet the accuracy requirements of the ESA increase by 10% even if the laser pulse energy is not increased significantly when the quantile is between 40% to 90%. The average increment of the laser pulse energy is 6.75 mJ which can increase the quantiles by 10% for the three orbits as a whole. When the laser pulse energies are set to 67.89, 73.71, and 75.98 mJ, the quantiles are up to 80%, which exceeds the percentage of bins (76.46%) for Aeolus without the impact of the SBR.

4.4 Uncertainties of wind observations resulting from an increased laser pulse energy

In Sect~~.~~ion 4.3, the zonal distributions of the required laser pulse energies were derived for different purposes. In order to offer a feasible proposal for the laser pulse energies of the new spaceborne DWLs, and the percentages of the bins that ~~can~~ meet the specific accuracy requirements when the laser energies reach~~ed~~ certain values were ~~figured out,~~determined as is shown in Table 3.

Considering the accuracy requirements of the ESA and the accuracy level of Aeolus and~~, while~~ taking the existing technical level into account, the laser energies of the two new spaceborne DWLs ~~are~~ were set to 70 mJ in this ~~paper~~study. In fact, the laser energy of 80 mJ has ~~been~~ already been required by the ESA in the ATBD (Reitebuch et al., 2018), and it has been achieved in the initial orbiting phase of the satellite. As is shown in Table 3, the percentages of the bins ~~which will~~that meet the accuracy requirements of the ESA are 77.19% and 74.71% for ~~orbit~~ the 15:00 and 12:00 orbits, respectively, which are close ~~equivalent~~ to the percentage of Aeolus without the impact of the SBR (76.46%). Moreover, ~~In addition, t~~the percentages of the bins are up to 89.04% and 77.34% for ~~orbit~~ the 15:00 and 12:00 orbits, so the accuracies of ~~of which~~ the ~~accuracy of~~ observations are equals to or exceed~~s~~ the accuracy level of Aeolus.

Table 3. Percentages of bins which will meet the specific accuracy requirements with certain laser pulse energies for spaceborne DWLs.

Accuracy requirements		Laser pulse energy (mJ)					
		50	60	70	80	90	100
ESA (%)[a]	Orbit 18:00	51.61	71.35	82.89	90.50	96.64	98.54
	Orbit 15:00	37.13	63.45	77.19	85.53	93.42	97.66
	Orbit 12:00	33.33	60.67	74.71	84.21	91.96	97.22
Aeolus (%)[b]	Orbit 15:00	0	19.44	89.04	99.42	100	100
	Orbit 12:00	0	16.67	77.34	96.78	100	100

[a] The percentage of bins which will meet the accuracy requirements of ESA when the laser energies reach the specific value.

[b] The percentage of bins which will reach the accuracy level of Aeolus in the corresponding bins when the laser energies reach the specific value.

~~Provided that~~For the three spaceborne DWLs opera~~teting~~ on the sun-synchronous orbits shown in Fig. 1, ~~and~~ the instrument parameters of Aeolus ~~keep~~ remain unchanged. As to the two new Aeolus-type spaceborne DWLs, the other instrument parameters are set ~~as~~ the same as those of Aeolus, except for the laser pulse energies of 70 mJ. The wind observation uncertainty distributions of the three spaceborne DWLs ~~are~~ were derived ~~as is~~and are shown in Fig. 8. Note that Fig~~s~~. 8 (a, b) ~~are~~ is identical to ~~those of~~ Fig~~s~~. 5 (a, b), ~~for that~~because both ~~of them are~~were obtained with laser energies of 60 mJ.

As is illustrated by~~in~~ Table 3, when the laser pulse energies of ~~three~~ the sawn-dusk, 15:00, and 12:00 spaceborne DWLs are 60, 70, and 70 mJ, respectively, the percentages of the bins ~~which~~ that meet the accuracy requirements of the ESA are close (71.35%, 77.19%, and 74.71%, respectively). And Fig. 8 illustrates that the bins that reach the ESA's accuracy requirements ~~are of high consistency in~~ have very consistent latitude and height distributions. By Compari~~sons~~ng among Fig. 8 (c–f) and Fig. 4, it can be seen ~~illustrate~~ that the wind observation accuracy is significantly improved~~promotes much~~ in the hemisphere that is less affect by the SBR. However, limited improvement ~~happens~~ occurs in the other hemisphere. ~~The fact~~This indicates that increasing the laser energy to 70 mJ cannot compensate ~~the~~ for the negative influence of the large amount of the SBR. By Compari~~sons~~ng ~~among~~ Fig. 8 (c–f) and Fig. 5 (c–f), it can be seen ~~show~~ that the wind observation accuracy is greatly improved when the laser pulse energy is increase~~d~~s from 60 mJ to 70 mJ. The fact that such improvements are obtained ~~with~~ for only a 10 mJ increase~~ment~~ in the laser pulse energy illustrates that the wind observation uncertainties are sensitive to the laser pulse energy~~ies~~ of the spaceborne DWLs. The average~~d~~ uncertainties of the two new spaceborne DWLs with a laser pulse energy~~ies~~ of 70 mJ in troposphere and stratosphere are 2.62 and 2.69 m/s respectively. Compared to the average~~d~~ uncertainties ~~with~~ for a laser pulse energy of 60 mJ, the difference in the uncertainties ~~is~~ are 2.96–2.62=0.34 m/s and 3.04–2.69=0.35 m/s

(a) (c) (e)

smaller, which indicates that when the laser pulse energies of the two new spaceborne DWLs are increased from 60 mJ to 70 mJ, the global average~~d~~ wind observation uncertainties ~~will~~ decrease by about 0.34 m/s under the impact of the maximum SBR conditions.

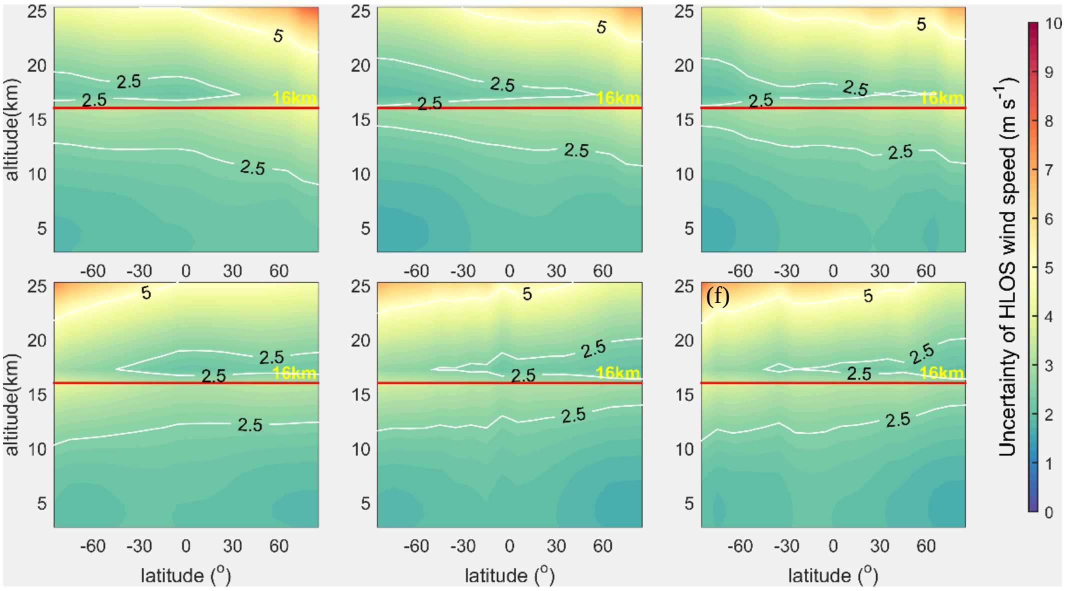

Figure 8. The zonal distributions of the wind observation uncertainties of the three spaceborne DWLs with the laser energy of 60 mJ for Aeolus , and with ~~the~~ a laser energy~~ies~~ of 70 mJ for the two new Aeolus-type spaceborne DWLs. The arrangement of the subgraphs corresponds to that of Fig. 2.

5 Summary and conclusions

The successful launch of Aeolus is significant for ~~people to~~ observ~~e~~ing the global wind field. Aeolus operates on the sun-synchronous dawn-dusk orbit to minimize the impact of the SBR on the accuracy of the wind observations. If ~~the~~ future spaceborne DWLs operate on other sun-synchronous orbits ~~for~~ to fulfil their specific observation purposes, the received SBR may become larger, which would lead to higher observation uncertainties. In general, for sun-synchronous orbits, ~~the~~ a spaceborne DWL ~~running~~ operating on ~~the~~ a dawn-dusk orbit (LTAN of 18:00) will receive the minimum SBR~~,~~; and ~~the~~ a spaceborne DWL ~~running~~ operating on ~~the~~ a noon-midnight orbit (LTAN of 12:00) will receive the maximum SBR. In this paper, the influence of the LTAN ~~crossing~~ of the sun-synchronous orbit on the wind observation accuracy ~~for~~ of Aeolus-type spaceborne DWLs was ~~studied~~investigated~~. And~~ based on two ~~the~~ spaceborne DWLs ~~running~~ operating on ~~three~~ sun-synchronous orbits with LTANs of ~~18:00, 1~~5:00~~,~~ and 12:00 ~~respectively were proposed~~combined with Aeolus. The method of increasing the laser pulse energ~~y~~ies of spaceborne DWLs was used to lower the observation uncertainties. Furthermore, ~~the~~ a method ~~to~~ of quantitatively designing laser pulse energy to meet ~~the~~ specific accuracy requirements was ~~also studied~~developed.

~~Assuming~~ For two new Aeolus-type spaceborne DWLs operatinge on ~~the~~ sun-synchronous orbits with LTANs of 15:00 and 12:00,~~.~~ t~~T~~he global distributions of the SBR illustrate that the increments of the average~~d~~ SBR range from 39 to 56 mW·m^{-2}·sr^{-1}·nm^{-1} ~~on the two new orbits~~ near the summer and winter solstices compared to that of the Aeolus under cloud-free skies~~, which will~~. This lead to the average~~d~~ uncertainty increments of 0.19 m/s ~~for 15:00 orbit~~ and 0.27 m/s for the 15:00

12:00 orbits, respectively. Considering that the impact of the SBR on the wind observations is minimal on a dawn-dusk orbit, and reaches the maximum on a noon-midnight orbit, the ~~phenomenon indicates the~~ selection of the LTAN of a sun-synchronous orbit~~s~~ will ~~make~~ result in a maximum difference of 0.27 m/s in the global average wind observation uncertainties ~~a maximum difference of 0.27 m/s~~ for the Rayleigh channel of Aeolus-type DWLs near the summer and winter solstices. Furthermore, the average global ~~averaged~~ uncertainty is 2.61 m/s ~~ies~~ without the impact of the SBR ~~is 2.61 m/s~~, and the average global ~~averaged~~ uncertaint~~ies~~y is 3.04 m/s under the worst SBR case~~s~~ ~~of~~for Rayleigh channel on the orbit with an LTAN of 12:00. Th~~e~~is fact illustrates that the maximum increase in the ~~averaged value of~~average global wind observation uncertainty ~~by about~~due to SBR is 3.04–2.61=0.43 m/s for Aeolus-type DWLs operating on ~~the~~ sun-synchronous orbits ~~due to SBR~~. In addition, the statistics show that 71.35% of the bins of Aeolus ~~can~~ meet the accuracy requirements of the ESA in the free troposphere and in the stratosphere near the summer and winter solstices. For the two new spaceborne DWLs, the percentages are 63.45% ~~for the orbit of 15:00~~ and 60.67% for the ~~orbit of~~ 15:00 and 12:00 orbits. Therefore, it is necessary to increase the laser pulse energies of the two new spaceborne DWLs to promote wind observation accuracy and to increase the percentage~~s~~ of bins ~~which~~that ~~could~~ meet accuracy requirements of the ESA. ~~On the other hand~~Moreover, the wind observation uncertainties are sensitive to the laser pulse energ~~ies~~y, and results ~~in~~of this ~~paper~~study show that the percentage~~s~~ of bins ~~which could~~that meet the accuracy requirements of the ESA would increase by 10% ~~with~~ when the laser pulse energy is increased by an~~only~~ average~~d~~ of only ~~increment of~~ 6.75 ~~mJ in laser pulse energies considering~~for the three orbits.

~~–~~To quantitatively design the required laser pulse energies of the new spaceborne DWLs ~~to~~ so that they meet the specific accuracy requirements, i.e., ~~to meet~~ the accuracy requirements of the ESA, or ~~to~~ reach the ~~similar~~ accuracy level of Aeolus, the relationship between the SNR and the uncertainty of the response function of the Rayleigh channel ~~is~~ was established based on ~~some~~ several assumption and simplifications~~,~~. ~~which is proven of~~This is demonstrated to have a wide feasibility by simulation experiments, ~~as~~which is shown in the Appendix. Finally, ~~the~~ a method ~~to~~ of deriv~~e~~ing the required laser energies according to the accuracy requirements is proposed.

~~According to the method, t~~The required energy is determined by temperature, pressure, wind uncertainty, SBR, and noise of instrument, and thus, the required laser pulse energies are different in different bins. Therefore, the laser pulse energies of the spaceborne DWLs should be determined ~~through~~ based on the statistics. ~~Considerations are given~~In order to reach ~~both of reaching~~ the accuracy level of Aeolus and ~~improving~~ improve the forecast results of the NWPs~~,~~ and taking the existing technical level of spaceborne DWLs into account, the laser pulse energies of two new spaceborne DWLs were~~are~~ set to 70 mJ, while other parameters ~~are~~ were the same as those of Aeolus. Based on the proposed parameter~~proposal~~s, 89.04% and 77.34% of the bins ~~can~~ reach the accuracy level of Aeolus ~~on~~ for the ~~two new~~15:00 and 12:00 orbits. ~~And~~ Moreover, the percentages of the bins that meet the ESA's accuracy requirements are 77.19% and 74.71% for the two new spaceborne DWLs, ~~of~~ which ~~values~~ are higher than that of Aeolus (71.35%), and are close~~ly equivalent~~ to the percentage ~~of~~for 76.46% ~~when~~ Aeolus when it is ~~are~~ free of the impact of the SBR. The average~~d~~ uncertainties of the two new spaceborne DWLs with laser pulse energies of 70 mJ in the free troposphere and stratosphere are 2.62 and 2.69 m/s, respectively, which perform better than that of Aeolus (2.77 m/s). Furthermore, when the laser pulse energies of the two new spaceborne DWLs increase from 60 mJ to 70 mJ, the average global ~~averaged~~ wind observation uncertainties ~~will~~ decrease by about 0.34 m/s under the impact of the maximum SBR. In summary, it is necessary to increase the laser pulse energies of the two new Aeolus-type spaceborne DWLs operating on ~~the~~ sun-synchronous orbits with LTANs of 15:00 and 12:00. The wind measurement accuracy ~~has been~~is greatly improved when the laser pulse energies are increased from 60 mJ to 70 mJ.

The essence of lowering the wind observation uncertainties of spaceborne DWLs by increasing the laser pulse energies is to increase the SNR of the received signal. Other methods can be used to improve the SNR of the received signal, such as enlarging the telescope aperture or reducing the vertical resolution. Once the quantitative relationship between these instrument parameters and the SNR is established, we can also quantitatively adjust these parameters according to ~~our~~ the accuracy requirements ~~as~~ using the method ~~shown~~ described in this paper.

Appendix

To build the relationship between the laser pulse energies and uncertainties of wind observations for Aeolus-type spaceborne DWLs, we derived the relationship between the response function and the SNR of the Rayleigh channel. According to Eq~~s~~. (3) and (4), the uncertainty of response function of Rayleigh channel can be written as follows based on the assumption that $N_A \approx N_B$ and $N_{S,A} \approx N_{S,B}$,

$$\begin{aligned}\sigma_{R_{ATM}} &= \frac{2}{(N_A+N_B)^2}\sqrt{N_B^2\left(N_A+N_{S,A}+N_{noise}^2\right)+N_A^2\left(N_B+N_{S,B}+N_{noise}^2\right)} \\ &\approx \frac{2}{4N_A^2}\sqrt{2N_A^2\left(N_A+N_{S,A}+N_{noise}^2\right)} \\ &= \frac{\sigma_A}{\sqrt{2}N_A}\end{aligned} \tag{A1}$$

According to Eq. (6), the SNR of the Rayleigh channel for spaceborne DWLs can be expressed as

$$\begin{aligned}SNR_{Ray} &= \frac{N_A+N_B}{\sqrt{N_A+N_B+N_{S,A}+N_{S,B}+2N_{noise}^2}} \\ &\approx \frac{2N_A}{\sqrt{2\left(N_A+N_{S,A}+N_{noise}^2\right)}} \\ &= \frac{\sqrt{2}N_A}{\sigma_A}\end{aligned} \tag{A2}$$

Therefore,

$$SNR_{Ray} \approx \frac{1}{\sigma_{R_{ATM}}} \tag{A3}$$

As is the equations derivation process shown in Sect~~.~~ion 3.2, the relationship between the SNR and the uncertainty of response function shown in Eq. (A3) is the basis to derive the relationship between the laser pulse energy and the wind observation uncertainty shown in Eq~~s~~. (10) and (11). However, Eq. (A3) is derived through assumption and simplifications, especially the assumption $N_A \approx N_B$, of which the values may be of large differences when the absolute values of HLOS wind speed are large. To test the correctness of Eq. (A3) in the actual atmosphere with variable wind speed, we verified the equation using reanalysis data, aerosol optical parameters database LIVAS and surface albedo database. The verification process is shown in Fig. A1.

The reanalysis data is were obtained from the 20th Century Reanalysis Project (Compo *et al.*, 2011). In the validation experiments, the monthly averaged 24 level profiles of the temperature, pressure, u- and v-components of the wind with 1°×1° spatial resolutions are were obtained from the reanalysis data. In this study, the reanalysis data for June 2015 and December 2015 are were used as the atmospheric conditions in summer and winter, respectively. As is shown in Fig. A1, the verification process of described by Eq. (A3) can be described as follows.:

(1) The off-nadir points of the spaceborne DWLs are obtained using orbit simulation software based on the orbit information of the spaceborne DWLs.

(2) The profiles of the temperature, pressure, wind speed, aerosol optical parameters, and surface albedo are interpolated into the off-nadir points.

(3) The SBR values of the off-nadir points are derived using the RTM libRadtran with the inputs provided in step (2).

(4) The profile values of N_A, N_B and $N_{S,A}$, $N_{S,B}$ are figured outdetermined using spaceborne DWL simulation system mentioned described in Section. 2.2 with the inputs of SBR and atmospheric conditions of the off-nadir points.

(5) The values of $\sigma_{R_{ATM}}$ and SNR_{Ray} are obtained using Eqs. (3), (4), and (6). In addition, according to the ADM-Aeolus ATBD Level 1B products (Reitebuch *et al.*, 2018), the noise of the detection chain for each measurement is 4.7 e$^-$/pixel. And There are 30 measurements are include in one observation, therefore, $C = 2N_{noise}^2 = 2 \times (4.7 \times 30)^2 = 39762$ in Eq. (10), which cannot beis not negligible.

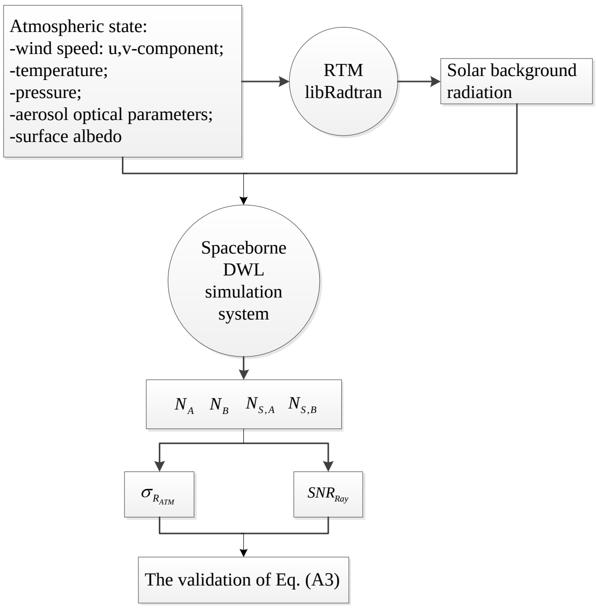

Figure A1. The verification process of Eq. (A3).

The scatters of $\sigma_{R_{ATM}}$ and $1/SNR_{Ray}$ are plotted to verify the accuracy of Eq. (A3), as is shown in Fig. A2. The spatial resolution of the reanalysis data is 1°×1°, so the earth Earth is divided into 1°×1° grids during the verification process, and one off-nadir point in each grid is selected as the verification point. Considering the SBR in summer and winter, and excluding some grid points with invalid data, a total of 28460 profiles are used in ~~this~~ the verification. Each profile contains 24 bins, and the verification uses 683040 scattered points.

In the verification, the HLOS wind components derived from u- and v-wind components ~~ranges~~ range from -73.02 to 33.14 m/s. Fig. A2 illustrates that the ~~scatter~~ points plot ~~between~~ of the reciprocal SNR ~~and~~ versus the uncertainty of the response function of the Rayleigh channel ~~is~~ plot very close to the ~~line~~ $y = x$ line, which demonstrates that the assumption and simplifications used in deriving the relationship between the laser pulse energy and the uncertainty of the wind observation are reasonable, and Eq. (A3) ~~is of~~ has a wide applicability and feasibility in the real atmosphere.

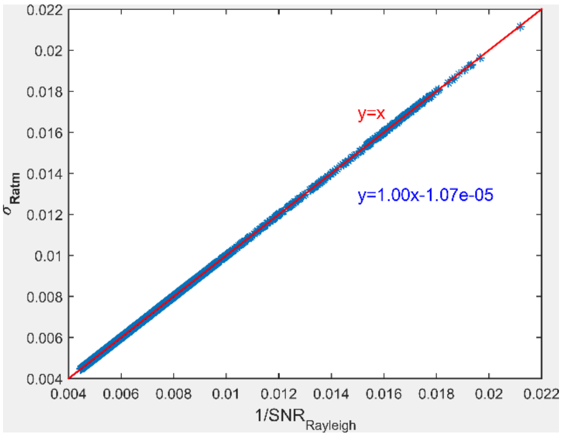

Figure A2. The scatter plot ~~between~~ of the reciprocal SNR versus the~~and~~ uncertainty of the response function of the Rayleigh channel and their first order fitting relationship.

The variables used in the verification of Eq. (A3) can ~~be~~ also be used in the verification of Eq. (11). The variable ~~of~~ $\partial v_{HLOS}/\partial R_{ATM}$ is also needed~~, which~~. It is ~~the~~ a function of temperature and pressure, and can be obtained through a pre-calculated lookup table. The verification results ~~of~~ for Eq. (11) are shown in Fig. A3.

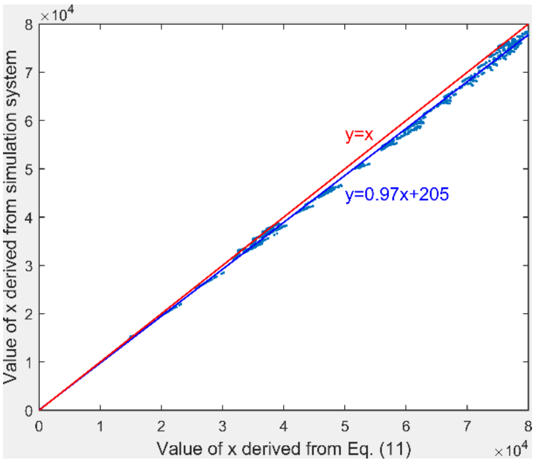

Figure A3. The scatter plot of the ~~values of~~ x values which are derived from Eq. (11) and simulation system~~ which~~. And x is the sum of N_A and N_B ~~respectively~~.

As is shown in Fig. A3, the fitting line of the ~~scatter~~points on the plot of ~~value~~ the x values derived from Eq. (11) ~~and~~ versus the values derived from the simulation system ~~is~~ plot very close to the ~~line~~ $y = x$ line. Furthermore, the residuals between the~~ scattered~~ points and the fitting~~ed~~ line are very small, which indicates the wide feasibility and applicability of Eq. (11). In addition, it ~~is noteworthy~~should be noted that the ~~scattered ~~points ~~of ~~in Fig. A3 ~~are ~~mostly ~~located ~~plot below the~~ line~~ $y = x$ line, which indicates that the ~~value of~~ x values calculated ~~by ~~using Eq. (11) ~~is ~~are smaller than the actual values. According to Section~~.~~ 3.3, the laser pulse energy is derived based on the equation $E_{new}/E_{Aeolus} \approx x2/x1$;~~.~~ a~~A~~nd $x1$ is obtained from the simulation system, which is regarded to be close to the real value. ~~The ~~A smaller $x2$ may lead to a smaller E_{new}, which is about 0.97 times ~~to ~~the real value.

Code and Data availability. The codes in this article are mainly compiled using matlab and are available upon request from the first author by email, zhang01020@hotmail.com. The databases used in this paper include: OMI database, which provided the latitude-averaged temperature, pressure, and ozone, can be accessed via anonymous ftp from toms.gsfc.nasa.gov/ pub/LLM_climatology; LIVAS database, providing the golabl aerosol optical properties with 1°×1° grid, offered by Dr. V. Amiridis from Institude for space applications and remote sensing, National observatory of Athens, and can be assessed from http://lidar.space.no a.gr:8080/livas/; the global LER database is available upon request from the authors, Dr. R. B. A. Koelemeijer from Air Research Laboratory, National Institute of Public Health and the Environment, robert.koelemeijer@rivm.nl; and the reanalysis data of 20th Century Reanalysis provided by the NOAA/OAR/ESRL PSD, Boulder, Colorado, USA, from their Web site at https://www.esrl.noaa.gov/psd/.

Author contributions. CZ, XS, and WL designed the studies; CZ built the simulation systems, performed the computation and analysis, and wrote the paper text; YS, ND, and SL provided important information on data delivery and processing. All authors engaged in discussions on studies, interpretation of results, as well as contribution to the finalization of the paper text.

Competing interests. The authors declare that they have no conflict of interest.

Acknowledgements. Thanks for the helpful discussions provided by Dr. Karsten Schmidt from DLR, Dr. Gert-Jan Marseille and Dr. Ad Stoffelen from Royal Netherlands Meteorological Institute in the building simulation system of Aeolus-type spaceborne DWLs. Thanks for the suggestions provided by Dr. Claudia Emde in running the libRadtran.

Financial support. This research was supported by National Natural Science Foundation of China (NSFC) (41575020).

References:

Amiridis, V., Marinou, E., Tsekeri, A., Wandinger, U., Schwarz, A., Giannakaki, E., Mamouri, R., Kokkalis, P., Binietoglou, I., Solomos, S., Herekakis, T., Kazadzis, S., Gerasopoulos, E., Proestakis, E., Kottas, M., Balis, D., Papayannis, A., Kontoes, C., Kourtidis, K., Papagiannopoulos, N., Mona, L., Pappalardo, G., Le Rille, O. and Ansmann, A.: LIVAS: a 3-D multi-wavelength aerosol/cloud database based on CALIPSO and EARLINET, Atmos. Chem. Phys., 15(13), 7127-7153, https://doi.org/10.5194/acp-15-7127-2015, 2015.

Baars, H., Geiß, A., Wandinger, U., Herzog, A., Engelmann, R., Bühl, J., Radenz, M., Seifert, P., Althausen, D., Heese, B., Ansmann, A., Martin, A., Leinweber, R., Lehmann, V., Weissmann, M., Cress, A., Filioglou, M., Komppula, M. and Reitebuch, O.: First results from the German CAL/VAL activities for Aeolus, The 29th International Laser Radar Conference, Hefei, China, 2019.

Compo, G. P., Whitaker, J. S., Sardeshmukh, P. D., Matsui, N., Allan, R. J., Yin, X., Gleason, B. E., Vose, R. S., Rutledge, G., Bessemoulin, P., Brönnimann, S., Burnet, M., Crouthamel, R. I., Grant, A. N., Groisman, P. Y., Jones, P. D., Kruk, M. C., Kruger, A. C., Marshall, G. J., Maugeri, M., Mok, H. Y., Nordli, Ø., Ross, T. F., Trigo, R. M., Wang, X. L., Woodruff, S. D. and Worley, S. J.: The Twentieth Century Reanalysis Project, Q. J. Roy. Meteor. Soc., 137(654), 1-28, https://doi.org/10.1002/qj.776, 2011.

Emde, C., Buras-Schnell, R., Kylling, A., Mayer, B., Gasteiger, J., Hamann, U., Kylling, J., Richter, B., Pause, C., Dowling, T. and Bugliaro, L.: The libRadtran software package for radiative transfer calculations (version 2.0.1). Geosci. Model Dev., 9(5), 1647-1672, https://doi.org/10.5194/gmd-9-1647-2016, 2016.

Flesia, C. and Korb, C. L.: Theory of the double-edge molecular technique for Doppler lidar wind measurement, Appl. Opt., 38(3), 432-440, 1999.

Hasinoff, S. W., Durand, F. and Freeman, W. T.: Noise-Optimal Capture for High Dynamic Range Photography, Proceedings of the IEEE Computer Society Conference on Computer Vision and Pattern Recognition, Los Alamitos, 553-560, https://doi.org/10.1109/CVPR.2010.5540167, 2010.

Heliere, A., Bezy, J. L., Bensi, P. and Ingmann, P.: System definition of the ESA Earth Explorer WALES mission, Sensors, Systems, and Next-Generation Satellites VI, Crete, Greece, 24-32, 2002.

Ishii, S., Baron, P., Aoki, M., Mizutani, K., Yasui, M., Ochiai, S., Sato, A., Satoh, Y., Kubota, T., Sakaizawa, D., Oki, R., Okamoto, K., Ishibashi, T., Tanaka, T. Y., Sekiyama, T. T., Maki, T., Yamashita, K., Nishizawa, T., Satoh, M. and Iwasaki, T.: Feasibility study for future space-borne coherent Doppler wind lidar, Part 1: Instrumental Overview for Global Wind Profile Observation, J. Meteorol. Soc. Jpn., 95(5), 301-317, https://doi.org/10.2151/jmsj.2017-017, 2017.

John E.: http://www.wmo-sat.info/oscar/requirements, Ids 311-313, 2009.

Koelemeijer, R., de Haan, J. F. and Stammes, P.: A database of spectral surface reflectivity in the range 335-772 nm derived from 5.5 years of GOME observations, J. Geophy. Res.-Atmos., 108(D2), 171-181, https://doi.org/10.1029/2002JD002429, 2003.

Liu, Z., Hunt, W., Vaughan, M., Hostetler, C., Mcgill, M., Powell, K., Winker, D. and Hu, Y.: Estimating random errors due to shot noise in backscatter lidar observations, Appl. Opt., 45(18), 4437-4447, https://doi.org/10.1364/AO.45.004437, 2006.

Ma, Z., Riishojgaard, L. P., Masutani, M., Woollen, J. S. and Emmitt, G. D.: Impact of different satellite wind lidar telescope configurations on NCEP GFS forecast skill in observing system simulation experiments, J. Atmos. Ocean. Tech., 32(3), 478-495, https://doi.org/10.1175/JTECH-D-14-00057.1, 2015.

Marseille, G. J. and Stoffelen, A.: Simulation of wind profiles from a space-borne Doppler wind lidar. Q. J. Roy. Meteor. Soc., 129(594A), 3079-3098, https://doi.org/10.1256/003590003769682183, 2003.

Marseille, G., Stoffelen, A. and Barkmeijer, J.: Impact assessment of prospective spaceborne Doppler wind lidar observation scenarios, Tellus A, 60(2), 234-248, https://doi.org/10.1111/j.1600-0870.2007.00289.x, 2008.

Masutani, M., Woollen, J. S., Lord, S. J., Emmitt, G. D., Kleespies, T. J., Wood, S. A., Greco, S., Sun, H. B., Terry, J., Kapoor, V., Treadon, R. and Campana, K. A.: Observing system simulation experiments at the National Centers for Environmental Prediction, J. Geophys. Res.-Atmos., 115(D7), https://doi.org/10.1029/2009JD012528, 2010.

Mcpeters, R., Kroon, M., Labow, G., Brinksma, E., Balis, D., Petropavlovskikh, I., Veefkind, J. P., Bhartia, P. K. and Levelt, P. F.: Validation of the Aura Ozone Monitoring Instrument total column ozone product, J. Geophys. Res.-Atmos., 113 (15). https://doi.org/10.1029/2007JD008802, 2008.

Nakajima, T. Y., Imai, T., Uchino, O. and Nagai, T.: Influence of daylight and noise current on cloud and aerosol observations by spaceborne elastic scattering lidar. Appl. Opt., 38(24), 5218-28, https://doi.org/10.1364/AO.38.005218, 1999.

Paffrath, U.: Performance assessment of the Aeolus Doppler wind lidar prototype, Doctor of Engineering, Ludwig-Maximilians-Universität München, 2006.

Reitebuch, O., Huber, D. and Nikolaus, I.: ADM-Aeolus ATBD Level 1B Product, European Space Agency, 2018.

Rennie, M.: CCN6 results: further Chain-of-Processors testing of L2B results and testing of CCN6 L2B processor algorithm updates, European Centre for Medium-Range Weather Forecasts, 2017.

Stoffelen, A., Marseille, G. J., Bouttier, F., Vasiljevic, D., de Haan, S. and Cardinali, C.: ADM-Aeolus Doppler wind lidar Observing System Simulation Experiment, Q. J. Roy. Meteor. Soc., 132(619B), 1927-1947, https://doi.org/10.1256/qj.05.83, 2006.

Stoffelen, A., Pailleux, J., Kallen, E., Vaughan, J. M., Isaksen, L., Flamant, P., Wergen, W., Andersson, E., Schtberg, H., Culoma, A., Meynart, R., Endemann, M. and Ingmann, P.: The atmospheric dynamics mission for global wind field measurement, B. Am. Meteorol. Soc., 86(1), 73, https://doi.org/10.1175/BAMS-86-1-73, 2005.

Stoffelen, A., Verhoef, A., Verspeek, J., Vogelzang, J., Marseille, G., Driesenaar, T., Risheng, Y., De Chiara, G., Payan, C., Cotton, J., Bentamy, A. and Portabella, M.: Research and Development in Europe on Global Application of the OceanSat-2 Research and Development in Europe on Global Application of the OceanSat-2 Scatterometer Winds: Final Report of OceanSat-2 Cal/Val AO project., KNMI, Royal Netherlands Meteorological Institute, de Bilt, the Netherlands, 2013.

Straume, A. G., Rennie, M., Isaksen, L., de Kloe, J., Marseille, G. J., Stoffelen, A., Flament, T., Stieglitz, H., Dabas, A., Huber, D., Reitebuch, O., Lemmerz, C., Lux, O., Marksteiner, U., Weiler, F., Witschas, B., Meringer, M., Schmidt, K., Nikolaus, I., Geiss, A., Flamant, P., Kanitz, T., Wernham, D., von Bismarck, J., Bley, S., Fehr, T., Floberghagen, R. and Parrinello, T.: ESA's space-based Doppler wind lidar mission Aeolus first wind and aerosol product assessment results, The 29th International Laser Radar Conference, Hefei, China, 2019.

Sun, X. J., Zhang, R. W., Marseille, G. J., Stoffelen, A., Donovan, D., Liu, L. and Zhao, J.: The performance of Aeolus in heterogeneous atmospheric conditions using high-resolution radiosonde data, Atmos. Meas. Tech., 7(8), 2695-2717. https://doi.org/10.5194/amt-7-2695-2014, 2014.

Tan, D. G. H., Anderson, E., De Kloe, J., Marseille, G., Stoffelen, A., Poli, P., Denneulin, M., Dabas, A., Huber, D., Reitebuch, O., Flamant, P., Le Rille, O. and Nett, H.: The ADM-Aeolus wind retrieval algorithms, Tellus A, 60(2), 191-205. https://doi.org/10.1111/j.1600-0870.2007.00285.x, 2008.

Vahlbruch, H., Mehmet, M., Chelkowski, S., Hage, B., Franzen, A., Lastzka, N., Gossler, S., Danzmann, K. and Schnabel, R.: Observation of squeezed light with 10-dB quantum-noise reduction, Phys. Rev. Lett., 100(3), 033602, https://doi.org/10.1103/PhysRevLett.100.033602, 2008.

Zhang, C. L., Sun, X. J., Zhang, R. W. and Liu, Y. W.: Simulation and assessment of solar background noise for spaceborne lidar, Appl. Opt., 57(31), 9471-9479, https://doi.org/10.1364/AO.57.009471, 2018.

Zhang, C. L., Sun, X. J., Zhang, R. W., Zhao, S. J., Lu, W., Liu, Y. W. and Fan, Z. Q.: Impact of solar background radiation on the accuracy of wind observations of spaceborne Doppler wind lidars based on their orbits and optical parameters, Opt. Express, 27(12), A936-A952, https://doi.org/10.1364/OE.27.00A936, 2019.

Zhang, R. W., Sun, X. J., Yan, W., Zhao, J., Liu, L., Li, Y., Zhang, C. L. and Zhou, J. H.: Simulation of frequency discrimination for spaceborne Doppler wind lidar (II): Study on the retrieval of atmospheric wind speed for Rayleigh channel based on Fabry-Perot interferometer, Acta Phys. Sin.-Ch. Ed., 63(14), 147-156. https://doi.org/10.7498/aps.63.140703, 2014.